An Adaptive Color Similarity Function Suitable for Image Segmentation and its Numerical Evaluation

Rodolfo Alvarado-Cervantes,[1] Edgardo M. Felipe-Riverón,[2*] Vladislav Khartchenko,[1] Oleksiy Pogrebnyak[2]

[1]Centro De Investigaciones Teóricas, Facultad De Estudios Superiores Cuautitlán, Universidad Nacional Autónoma De México, Primero De Mayo S/N Campo 1, Cuautitlán Izcalli, México

[2]Centro de Investigación en Computación, Instituto Politécnico Nacional, Juan De Dios Bátiz W/N, Col. Nueva Industrial Vallejo, P.O. 07738, México

Abstract: In this article, we present an adaptive color similarity function defined in a modified hue-saturation-intensity color space, which can be used directly as a metric to obtain pixel-wise segmentation of color images among other applications. The color information of every pixel is integrated as a unit by an adaptive similarity function thus avoiding color information scattering. As a direct application we present an efficient interactive, supervised color segmentation method with linear complexity respect to the number of pixels of the input image. The process has three steps: (1) Manual selection of few pixels in a sample of the color to be segmented. (2) Automatic generation of the so called color similarity image (CSI), which is a gray level image with all the gray level tonalities associated with the selected color. (3) Automatic threshold of the CSI to obtain the final segmentation. The proposed technique is direct, simple and computationally inexpensive. The evaluation of the efficiency of the color segmentation method is presented showing good performance in all cases of study. A comparative study is made between the behavior of the proposed method and two comparable segmentation techniques in color images using (1) the Euclidean metric of the a* *and* b* *color channels rejecting* L* *and (2) a probabilistic approach on* a* *and* b* *in the CIE L*a*b* color space. Our testing system can be used either to explore the behavior of a similarity function (or metric) in different color spaces or to explore different metrics (or similarity functions) in the same color space. It was obtained from the results that the color parameters* a* *and* b* *are not independent of the luminance parameter* L* *as one might initially assume in the CIE L*a*b* color space. We show that our solution improves the quality of the proposed color segmentation technique and its quick result is significant with respect to other solutions found in the literature. The method also gives a good performance in low chromaticity, gray level and low contrast images.*

INTRODUCTION

Image segmentation consists of partitioning an entire image into different regions, which are similar in some predefined manner.[1,2] Segmentation is an important feature of human visual perception, which manifests itself spontaneously and naturally. It is an important and difficult task in image analysis and processing. All subsequent steps, such as object recognition depend on the quality of segmentation.[1–3]

Color is an effective and robust visual feature to differentiate objects in an image. It is an important source of information in the segmentation process and may in many cases be used as a unique feature to segment objects of interest.[3]

At present, a large number of segmentation techniques are available for color images, but many of them are monochromatic methods applied on the individual planes in different color spaces where the results are combined later in different ways.[4] A common problem with this approach is that when the color components of a particular pixel are processed separately, the color information is so scattered in its components that much of the color information is lost.[3–6]

In this work, an adaptive color similarity function defined in a modified hue-saturation-intensity (HSI) color space is presented, which can be used directly as a metric to obtain pixel-wise segmentation of color images among other applications. As a direct application we present a very efficient interactive, supervised color segmentation method with linear complexity respect to the number of pixels of the input image, together with its characterization and evaluation. It basically relies on the calculation of a color similarity function for every pixel in a red-green-blue (RGB) 24-bit true color image. The color information of every pixel is integrated as a unit thus avoiding color information scattering.

The three color components of every pixel in RGB color model transformed to a modified HSI color model are integrated in two steps: in the definitions of distances in hue, saturation and intensity planes $[\Delta_h, \Delta_s, \Delta_i]$ and in the construction of an adaptive color similarity function that combines these three distances assuming normal probability distributions. To obtain a consistent color model for direct color comparisons, some modifications to the classical HSI color space were necessary. These modifications eliminated the discontinuities occurring in the red hue (in 0° and 360°) and the problems associated with them.

One weakness in the classical characterization of the achromatic region as presented in Plataniotis and Venetsanopoulos (2000) is its poor performance in the border regions of achromatic and chromatic zones, both in low and high brightness. This is due to the fact that the commonly used HSI color model does not take into account the human visual response at low and high brightness. Human vision has a nonlinear perceptual response to luminance.[7] We deal with this problem by modifying the saturation value of every pixel by a factor that reflects the human exponential response to brightness.

For some time, the development of segmentation algorithms attracted remarkable consideration compared with the relatively fewer efforts spent on their evaluation and characterization.[8–11] Since none of the proposed automatic segmentation algorithms published is generally applicable to all types of images and different algorithms are not equally suitable for particular applications, the performance evaluation of segmentation algorithms and its characterization are very important subjects in the study of segmentation.[9]

For a long time the evaluation was limited to few real images acquired from a particular application, which has the advantage that they are closer to reality, although its intrinsic random nature makes them unsuitable for analytical evaluation.[8,9,12] Many undetermined characteristics of those images make them practically impossible to be used to compare different segmentation techniques because many phenomena are mixed, which makes it difficult to study each one's influence individually.[9] Another problem comes from the lack of a ground truth (GT) which has to be obtained from "experts" whose results have intrinsic differences. This subjective and imprecise procedure is not appropriate for quantitative evaluation.[8,12]

So far segmentation evaluation methods can be divided into two groups: analytical and empirical. The analytical methods directly inspect and evaluate the segmentation algorithms themselves analyzing their principles and properties. The empirical methods indirectly judge the efficiency of segmentation algorithms applying them to test images and measuring the quality of the results.[9–11]

Several empirical methods have been proposed; the great majority of them can be classified as one of two types: goodness methods and discrepancy methods. In the first category, some desirable properties of segmented images, are often established according to human intuition, and measured by "goodness parameters". The performances of the segmentation algorithms are judged by the values of goodness measures. In the second group, the GT that presents the ideal or expected segmentation result must first be found. The actual segmentation results obtained by applying a segmentation algorithm are compared with the reference to count their differences. The performances of the segmentation algorithms under investigation are then estimated according to discrepancy measures.[8–11]

To evaluate and characterize our system, we generated synthetic color images with the associated GT. The synthetic images where designed to evaluate the efficiency of achieved color information from given segmentation algorithms. By the use and analysis of receiver operating characteristic (ROC)[13] curves and graphs, we obtained some proper characteristics of the segmentation method under study such as its stability related to the threshold selection and to the selection of an appropriate number of pixels required by the color samples.

The rest of the article is organized as follows: Previous Works section briefly reviews previous works in the field. In Description of the Method section, the proposed method is described in detail. Some results on real and low contrast images are presented and discussed in Results on Real and Low Contrast Images section. In the next section, the design and generation of synthetic images for the evaluation and characterization of the segmentation method are explained and discussed. Also Benchmark Testing section presents a comparative study between our method and two different implementations in the CIE $L*a*b*$ color space: (1) Minimum Euclidean Distance of $a*$ and $b*$ channels discarding $L*$ and (2) A

probabilistic approach on $a*$ and $b*$ channels. Concluding remarks are drawn in Conclusions section.

PREVIOUS WORKS

In recent years, considerable effort has been devoted to the problem of color segmentation in digital images given its importance and potential. Until recently, the majority of published approaches for the segmentation of color were based on monochromatic techniques applied to each color component of the image in different color spaces (RGB or other) and in different ways to produce a color composite. These approaches have an inherent problem of significant loss of color information during the process.[4] Currently available approaches and techniques in image segmentation vary widely: those based on mathematical morphology,[14] clustering in $L*a*b*$ color space,[15] computational topology,[16] biogeography based optimization,[17] neutrosophic sets,[18] multi-scale roughness measures,[19] comprehensive learning particle swarm optimization,[20] wavelets,[18,21,22] quaternions,[23] among others, but it is still an open problem.

Proper selection of the color space for color image processing is a very important aspect to be taken into account.[5] The representation in the RGB color space has several known drawbacks[5] but it is used in paper[23] in a novel form using quaternions. Several works[15,17,18,21] use CIE $L*a*b*$ or $L*u*v*$ color spaces, which have some advantages, such as the separation of lightness information (L), as well as handling the chromatic color similarity as the Euclidean distance between the independent channels $a*b*$ (or $u*v*$). These representations have the disadvantage that when managing the information of saturation and hue jointly in $a*b*$ (or $u*v*$) channels, it is difficult to predict whether the similarity is due to some/ one of these variables. In this article we present an improved color HSI space that keeps concordance with human color perception while eliminating known discontinuities of the classic HSI color space.

A comparative study[24] between several perceptually uniform color spaces (specifically: $L*a*b*$, $L*u*v*$ and Rlab) are presented in order to establish which color space is better for the segmentation of natural images. To perform the comparison, an empirical discrepancy method is used. This method needs a GT as "ideal" model of segmentation and calculates how the segmentation approaches this "ideal." The used ideal segmentation was made by different people on the Berkeley Segmentation Dataset. Only color information was used for comparative testing and excluded others. In the benchmark, two approaches were used: (1) supervised classification of pixels and (2) unsupervised classification using K-means. As a reference the threshold operator of the intensity image in RGB was used.

As a result they conclude that with the color space $L*u*v*$, the best results was obtained in both average discrimination capabilities and speed of processing.

Segmentations assessments made by individuals have intrinsic differences due to subjective errors to assess the significance of objects in the scene.[25] As for the method of assessing results, one can see that the results taken as ideal in the Berkeleýs dataset differ for different evaluators; the authors do not mention how they integrated the different segmentations for their ideal model of segmentation.

A semi-automatic segmentation algorithm for natural images is presented in ref. 26. The user first selects different regions of interest using simple scribbles and apart from them the whole image is segmented automatically. To achieve this task, weighted distances from the scribbles are calculated. The weighting is obtained starting from a number of Gabor filters to locate texture in the image.

In this method, the minimum geodesic distance were calculated considering only changes in luminosity as a weighting factor. The color similarity function proposed could be integrated in the calculation of the weights and in this way might improve their results, making the geodesic distance sensitive to homogeneity of color and not only to luminance.

Bai and Sapiro present a semi-automatic algorithm for natural images and video segmentation.[27] Their technique is based on calculating a weighted geodesic distance from every pixel to user-generated scribbles. Scribbles given by the user are much simplified compared to others systems because the user only needs to draw a line that crosses the region of interest. Their system can handle partial occlusions.

Weights for the geodesic distance are calculated according to changes in the probability that the pixel belongs to the object of interest. In this work, this probability is calculated from scribbles made by the user in the $L*u*v*$ color space. The color model and similarity function proposed in this article could also be integrated into this system. The weights could be calculated according to the gradient of the color similarity function.

Rother *et al.* present a semi-automatic segmentation method for objects of interest in complex backgrounds.[28] The method integrates information from homogeneous regions and edges. The segmentation is performed by minimizing an energy function where the information of the homogeneous regions and the edges are integrated. The work uses the RGB color space and Gaussian Mixture models for each pixel. As input from the user, the algorithm only needs a roughly frame of the object of interest. From this input, it is inferred that the square is located at the background and the object is contained in the box. A comparative study of the state of the art from different commercial semi-automatic systems is done. It is shown how their method requires less effort from the user.

Vaitkus and Várady present an image segmentation algorithm based on tools from computational algebraic topology and Morse theory.[16] They assign a quantity called persistence to its topological features, measuring their lifetime in the construction. In combination with concepts from Morse theory, they construct and simplify a watershed type segmentation of the complex. For color images, they apply a general algorithm on the

neighborhood graph of the point cloud representing the image in color space, which is filtered by Gaussian density estimation.

A biogeography based optimization approach for automatic color segmentation is proposed by Gupta et al.[17] Biogeography is the study of the geographical distribution of biological organisms, which is basically an evolutionary process that achieves information sharing by species migration. They use clusters in the L*a*b* color space (homogeneous regions) as habitats that are modified over time by rules of the field of biogeography. The optimization algorithm is similar to learning particle swarm optimization with some differences in their rules such as not to create children.

A novel method of automatic segmentation using neutrosophic sets representation and multi-resolution wavelet transformation analysis[18] is presented by Sengur and Gao. It uses both the color information (in the L*u*v* color space) and texture segmentation. Wavelet analysis allows the characterization of texture and a value of entropy to be obtained, which is used in the characterization of the color image with neutrosophic sets. Each pixel of the image is represented as a neutrosophic set, operations defined in this field being applicable.

Yue et al. present a multi-scale roughness measure based on simulating human vision.[19] They applied theories of linear scale-space and rough sets to generate the hierarchical roughness of color distribution on multiple scales. The segmentation algorithm is based on multi-scale roughness measure applied to color histograms. They proposed the roughness entropy for scale selection based on information variation.

An automatic segmentation method based on fuzzy sets and comprehensive learning using particle swarm optimization[20] is presented by Puranik et al. Fuzzy sets are defined on the hue-saturation-luminosity color space. During the search process, a population member tries to maximize a fitness criterion at every iteration, which is a high classification rate and small number of rules. Finally, the particle with the highest fitness value is selected as the best set of fuzzy rules for image segmentation.

Huang et al. address the problem of image segmentation under the paradigm of clustering-then-labeling.[5] They present an improved clustering algorithm, which could maintain good coherence of data in feature space and is used to do clustering on the L*a*b* color feature space of pixels. Rather than calculate the characteristics of each pixel, they are computed from atomic regions with homogeneous color characteristics called super-pixels. Image segmentation is straightforwardly obtained by setting each pixel with its corresponding cluster.

In ref. 23 Shi and Funt present a method using quaternion representation of color to segment the image into regions with similar color and texture. The advantage of using quaternion arithmetic is that a color can be represented and analyzed as a single entity. Each color component RGB input image is matched to each imaginary basis i, j, k of the quaternion that represents each pixel in the image. The real component of the quaternion is related to texture.

Celik and Tjahjadi present an unsupervised color image segmentation algorithm, which uses multi-scale edge information and spatial color content.[21] The multi-scale edge information is extracted using the dual-tree complex wavelet transform. Binary morphological operators are applied to the edge information to detect seed regions. The segmentation of homogeneous regions is obtained using region growing followed by region merging in the CIE L*a*b* color space.

A database[25] containing GT from segmentations produced manually by a group of people from a wide variety of color natural scenes is presented by Martin et al. The authors define two related error measures that quantify the consistency between segmentations of different granularities. This measure permits comparisons to be made between segmentations made by people and segmentations of the same scene made by the computer.

Kim et al. propose a color modeling in HSI color space considering intensity information by adopting the B-spline curve fitting to make a mathematical model for statistical characteristics of a color with respect to intensity.[29] The statistical characteristics contain the mean and standard deviation of hue and saturation with respect to intensity. The proposed algorithm was successfully applied to color images under various illumination conditions.

Harun et al. present a technique for segmenting acute leukemia images.[30] The segmentation technique segments each leukemia image into two regions: blast and background. In their approach, the segmentation is based on both HSI and RGB color spaces. The performance comparison between the segmentation algorithms is carried out to choose a better color image segmentation for blast detection. Their results show that the segmentation based on HSI color space has successfully segmented the acute leukemia images while removing background noise.

A color image segmentation scheme based on unsupervised pixel classification is presented by Macaire et al. in Ref. 31. When color points of different regions in the image produce a single cluster in the color space, the scheme splits this cluster into sub-populations of color-points defined by color-domains. For this purpose, the connectedness and the color homogeneity properties of color-subsets of pixels are analyzed in order to construct the classes, which correspond to the actual regions in the image.

The first comprehensive survey[9] on evaluation methods of image segmentation is compiled by Zhang. It brings a coherent classification of existing methods at that time. Progress made in the subject during the 5 years after the first survey is presented in Ref. 10. Another actualization is presented five years later[11] embracing together the principal methods of segmentation evaluation available up until 2007.

Chabrier et al. present a comparative study of 14 evaluation criteria of supervised image segmentation methods by generating edges.[32] The study was done in two parts: (1) evaluation with synthetic images to characterize the

general behavior of the algorithm that is complemented by (2) an assessment over a selection of real color images. To obtain the GT from different people's segmentations, the authors mention that their propositions were merged but do not give details of how they accomplished it.

A comprehensive survey on unsupervised methods of segmentation evaluation is presented in Ref. 8. Zhang *et al.* propose a hierarchy of published methods at that time by summarizing the main branches and locating the group of unsupervised methods on it. They mention its advantages, such as no requirement for GT to obtain quantitative results. They also propose the main lines of future research for this kind of methods.

A way to design synthetic images and a corresponding GT for evaluating segmentation algorithms is presented by Zhang and Garbrands.[12] The authors introduce a general framework and general design considerations. They also present a system for generating synthetic images in shades of gray taking into account their design considerations. The behavior of a segmentation method in gray images using a threshold operator is studied and some remarks are obtained.

DESCRIPTION OF THE METHOD

The segmentation method proposed in this article relies on the calculation of a color similarity function for every pixel in a RGB 24-bit true color image to form what we call a color similarity image (CSI), which is a gray level image. A true color image usually contains millions of colors, and many thousands of them represent the same perceived color of a single object due to the presence of additive noise, lack of definition between color borders and regions, shadows in the scene, the spatial resolution of the human vision system, and so forth.[1–3] The proposed color similarity function allows the clustering of the many thousands of colors representing the same perceived color in a single gray output image. The CSI is then automatically thresholded, and the output can be used as a segmentation layer or template, or it can be modified previously with morphological operators to introduce geometric enhancements if they are needed. The generation of a CSI only requires calculating Eq. (1) (below) for every pixel in the RGB input image. Thus, the complexity is linear with respect to the number of pixels in the source image and for that reason is inexpensive computationally.

First, we compute the color centroid and color standard deviation of a small sample consisting of a few pixels (less than 15 pixels per color as average) of the desired color. The computed centroid represents the desired color to be segmented using the technique we designed for that purpose. Then, our color similarity function uses the color standard deviation calculated from the pixel sample to adapt the level of color scattering in the comparisons. The result of a particular similarity function calculation for every pixel and the color centroid (meaning the similarity measure between the pixel and the representative

color value) generates the CSI. The generation of this image is the basis of our method and preserves the information of the color selected from the original color image. This CSI is a discrete representation in the range [0–255] of a continuous function whose values are in the normalized range [0–1]. The CSI can be thresholded with any automatic threshold method. To obtain the results presented in this work we used Otsu's method.[33,34]

To generate a CSI we need: (1) A color image in RGB 24-bit true color format and (2) A sample of arbitrarily selected pixels forming a sample of the color desired to be segmented. From this sample of pixels, we calculate the statistical indicators according to our modified HSI color model, which can be consulted in Alvarado (2006). This information is necessary to adapt the color similarity function in order to obtain good results. To obtain the CSI, we calculate for every pixel (i,j) in the image the following color similarity function S [Eq. (1)].

$$S_{i,j} = e^{\left(\frac{-\Delta_h^2}{2\sigma_h^2}\right)} * e^{\left(\frac{-\Delta_s^2}{2\sigma_s^2}\right)} * e^{\left(\frac{-\Delta_i^2}{2\sigma_i^2}\right)} \tag{1}$$

where Δ_h is the hue distance between hue (i, j) and the average_hue; Δ_s is the saturation distance between saturation (i,j) and the average_saturation; Δ_i is the intensity distance between intensity (i, j) and the average_intensity; σ_h is the hue standard deviation of the sample; σ_s is the saturation standard deviation of the sample; σ_i is the intensity standard deviation of the sample. In Eq. (1), the color information is integrated giving high importance to small perceptual changes in hue, as well as giving wide or narrow tolerance to the intensity and saturation values depending on the initial sample, which is representative of the desired color to be segmented.

The statistical values needed in Eq. (1) are calculated as follows[3]:

$$\text{saturation\_average} = S_c = \frac{1}{n} \sum_{i=1}^{n} \text{saturation}(i)$$

$$\text{Intensity\_average} = I_c = \frac{1}{n} \sum_{i=0}^{n} \text{intensity}(i)$$

$$\text{Hue\_standard\_deviation} = \sigma_h = \sqrt{\frac{\sum_{i=1}^{n} \Delta^2_h(i)}{n}}$$

$$\text{saturation\_standard\_deviation} = \sigma_s = \sqrt{\frac{\sum_{i=1}^{n} \Delta^2_s(i)}{n}}.$$

$$\text{intensity\_standard\_deviation} = \sigma_i = \sqrt{\frac{\sum_{i=1}^{n} \Delta^s_i(i)}{n}}.$$

where n is the number of pixels in the sample.

The common disadvantages attributed to the HSI color space such as the irremovable singularities of hue in very low saturations or the periodical nature of hue,[4] which is lost in its standard representation as an angle $\in [0°, 36°]$,

are overcome in our technique using vector representation in $\Re^2$, in the separation of chromatic and achromatic regions, and in the definition of the $\Delta_h, \Delta_s, \Delta_i$. Distance details can be consulted in Ref. 3.

Two modifications on standard HSI color space were necessary in order to create a consistent model to represent colors and color centroids:

1. Representation of hue. Instead of standard representation of hue as an angle in the range [0°–360°], hue is represented here as a normalized vector in $\Re^2$ (with magnitude 1 or 0). This representation has at least three advantages compared to an angle in the range [0°–360°]: (a) the existing discontinuity in 360° and 0° is eliminated; (b) the average hue of a group of pixels can be understood as the resulting angle of a vector addition of the color pixels in the chromatic region of the sample, giving a simple manner to calculate the average hue; (c) setting magnitude to 0 or 1 works as a flag intended for distinction between chromatic or achromatic regions.
2. Separation of chromatic and achromatic regions. The separation of the region as described in Ref. 7 is used to calculate the average hue and Δ_h. Once Δ_h, Δ_s, and Δ_i have been calculated this distinction is no longer necessary because in the formulation of $S_{i,j}$ [Eq. (1)] all the cases of color comparison between zones are accounted for, and it is a simple matter to maintain consistency. The use of Gaussians in the definition of $S_{i,j}$ [in Eq. (1)] reflects our belief that the color model modifications proposed in this article allow normal distributions of the color characteristics in this modified HSI color space according to the visual experience of color similarity.

Pixel Sample Selection

The pixel sample is a representation of the desired color(s) to be segmented from a color image. The selection of the pixel sample is the only step to be left up to the user. From this pixel sample, two values are calculated to feed our segmentation algorithm: the color centroid and a measure of the dispersion from this centroid, in our case the standard deviation. These two values are represented according to our modified HSI model.[3]

If only one pixel is taken, its color would represent the color centroid, and would produce dispersion equal to zero, giving a Dirac delta in the calculation of Eq. (1). This means that the similarity function would be strictly discriminative to the pixel color. This is not the general intention of segmenting color images which usually contain millions of colors, many thousands of them are due to additive noise. Thus, we used a small value for dispersion equal to 0.001 in the case of one pixel per sample.

If another pixel is additionally taken, the centroid of both and their standard deviation are then obtained to feed our algorithm. So when an additional pixel is selected, it must be taken from a region which was not or was poorly segmented when the first pixel was used. This means that in order to obtain good results the pixels for the sample should be taken from the color regions in such a form that they must constitute a good representation of the color variations in the region.

We have found that if more and more pixels are added to the sample, the corresponding centroid of the area to be segmented increases in accuracy. Here, we may enforce having a relatively small representative sample of the color area to segment. Beyond a given number of well-selected pixels in the sample, increasing them does not affect sensibly the segmentation quality because adding more pixels to the sample of approximately the same perceived color does not affect the statistical estimators to feed the algorithm in a sensible manner. The pixels of the sample are easily selected by the user from a (zoomed) square of 21 by 21 image pixels with a click of the mouse centered on the region whose color the user desires to segment. Each pixel of this (image) square is enlarged by 10 in both directions (x and y), that is, it is composed of 100 pixels of the same color.

The Achromatic Zone G

The achromatic zone G is the region in the HSI color space where no hue is perceived by a human. This means that color is perceived only as a gray level because the color saturation is very low or the intensity is either too low (near to black) or too high (near to white).

Given the three-dimensional HSI color space, the classical achromatic zone G is defined as the geometric union of the points inside the cylinder created by the zone Saturation < threshold_1 and the two cones Intensity < threshold_2 and Intensity > threshold_3. Pixels inside this region are perceived as gray levels (Fig. 1 left). Usually, threshold_1 and threshold_2 are equal to 10% and threshold_3 is equal to 90%.

In order to model the human visual response better in the abrupt corner regions near the union zones of the two cones with the cylinder of the singularity zone G, as presented in Refs. 2,3, we found that it is convenient to modify the characterization of the HSI color model for colors belonging to regions with very low or very high brightness as shown in Fig. 1 (left). In order to adjust zone G to a better model nearer to the human response to brightness, we introduced an exponential function with three parameters to define the improved singularity of zone G: saturation threshold (st), inflection point (ip), and Influence, as shown in Fig. 1 (right).[35]

Then, the saturation image will be affected now by a factor calculated from inflection point (ip) and Influence for every pixel (P) as shown in Eq. (2):

$$\text{New\_Saturation\_}(P) = \text{Pos}$$
$$\left(1 - \text{Influence} * (e-1)^{2*\text{abs}(ip - \text{Intensity}(P))}\right) \quad (2)$$
$$* \text{Saturation}(P)$$

where Influence is a parameter representing the degree of affectation of the exponential factor to the saturation attribute for every pixel; Pos() is a function that returns the input argument if it is positive and zero otherwise; abs() represents the
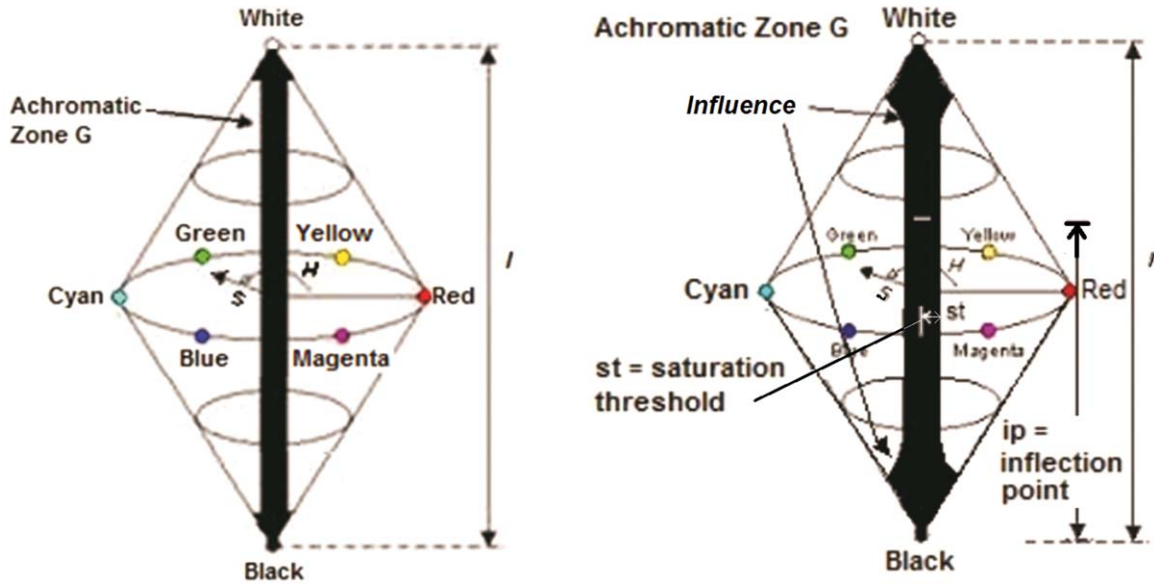
Fig. 1. The classic achromatic zone (left); the new achromatic zone *G* (right).

absolute value function and Intensity() is defined as an average of the RGB channels in Eq. (4) below. After calculating the New_Saturation values for the source image, it is thresholded with the saturation threshold (st) to obtain the effects of the improved achromatic zone *G*.

The inflection point (ip) is used to modify the point where the affectation of the exponential function begins in the new saturation calculation. It makes more or less sensitive the low or high levels of illumination. For example, a level of 0.5 indicates that the influence of the exponential function is the same in the regions of low and high illumination. A level of 0.6 indicates that the exponential function affects the low illumination regions more.

We found good performance with the parameters empirically determined in the following ranges: st ϵ [0.07, 0.1], ip ϵ [0.5, 0.6], and Influence ϵ [1, 1.5].

Calculation of Average Hue

In order to obtain the average of the hue (H_m) of several pixels from a sample, we took advantage of the vector representation in $\Re^2$. Vectors that represent the hue values of individual pixels are combined using vector addition. From the resulting vector, the average hue corresponding to the angle of this vector with respect to the red axis is obtained. Thus, H_m is calculated in the following manner:

For every pixel $P(x,y)$ in the sample, the following $\Re^3$ to $\Re^2$ transformation is applied:

$$V_1(p) = \begin{bmatrix} 1- & \cos(\pi/3)- & \cos(\pi/3) \\ 0 & \sin(\pi/3)- & \sin(\pi/3) \end{bmatrix} * \begin{bmatrix} R \\ G \\ B \end{bmatrix} = x\begin{bmatrix} x \\ y \end{bmatrix}$$

$$\text{if } P \notin G$$

(3)

and

$$V(P) = V_1(P)/|V_1(P)|;$$

in another case:

$$V(P) = \begin{bmatrix} 0 \\ 0 \end{bmatrix} \quad \text{if } P \in G$$

where $V(P)$ is the normalized projection of the RGB coordinates of the pixel P to the perpendicular plane to the Intensity axis of the RGB cube when the x axis is collinear to the Red axis of the chromatic circle. Conversely, G (see Section 3) represents the achromatic zone in the HSI space and $[RGB]^t$ is a vector with the color components of the pixel in the RGB color space. To carry out this, the following code is executed:

```
Vector.x = 0;
                Vector.y = 0;                       //initialize vectors
 For (i = 1; i < = n; i++)                 //for every pixel in the sample do
    { Vector.x = Vector.x + V(i).x;   //x-component of the accumulated vector
    Vector.y = Vector.y + V(i).y;}    //y-component of the accumulated vector
           Vs = [ Vector.x Vector.y] ;           //Accumulated vector
```

In this code we have a vector in $\Re^2$, which accumulates the vector additions as index i increments. Each of the vectors being added correspond to the previous $\Re^3$-to-$\Re^2$ transformation for every pixel in the sample made at step 1.

The angle of the accumulated vector (V_s) with respect to the x axis is the average hue:

$$H_m = \text{angle}(V_s, 0)$$

where 0 represents the Red axis.

Using the vector representation of Hue obtained by the $\Re^3$-to-$\Re^2$ transformation of RGB space points expressed in Eq. (2), the hue distance Δ_h between two color pixels or color centroids C_1 and C_2, can be calculated as follows:

$$\Delta_h(C_1, C_2) = |V_1 - V_2| \quad \text{if } C_1 \text{ and } C_2 \notin G$$
$$= 0 \quad \text{if } C_1 \text{ or } C_2 \notin G$$

where G is the achromatic region; V_1 and V_2 are the vectors in $\Re^2$ calculated with the transformation on C_1 and C_2 given in Eq. (2).

In our modified HSI color space, to each color tone of a chromatic pixel a vector in $\Re^2$ corresponds with amplitude equal to 1 and an angle (to the red axis) equal to the hue in the conventional HSI color space. In these conditions, when $|V1 - V2|$ is very small and the vectors are not near to the area of discontinuities of the conventional HSI color space ($0°$ and $360°$) then $|V1 - V2|$ tends to be equal to the angle (in radians) between the V1 and V2 vectors, that is, the difference in hue in the conventional HSI color space. Thus, our proposed distance distinguishes the different hues at least as well as it does the angular distance in the conventional HSI color space. We have done tests on real and synthetic images in different regions of color and in all of them the distance $|V1 - V2|$ appears to be effective in distinguishing colors with different hue throughout the proposed color space.

Saturation Distance and Intensity Distance

The saturation distance and the intensity distance can be calculated using the standard conversion equations for saturation and intensity from RGB to HSI space,[1,2] normalized in the range [0, 1] [Eq. (4)]:

$$\text{saturation}(P) = 1 - \left[\frac{3}{R+G+B} \min(R, G, B) \right].$$
$$\text{intensity}(P) = \frac{1}{3}(R+G+B) \tag{4}$$

In Eq. (4), we defined the saturation equal to zero in the case of black.

The Euclidean distance was used to define the saturation distance Δ_s and intensity distance Δ_i between two pixels or color centroids. The saturation distance Δ_s and the intensity distance Δ_i between two pixels or color centroids are defined as:

$$\Delta_s = \text{abs}[\text{saturation}(C_1) - \text{saturation}(C_2)], \text{ and}$$
$$\Delta_i = \text{abs}[\text{intensity}(C_1) - \text{intensity}(C_2)],$$

where C_1 and C_2 are color pixels or color centroids, respectively, in RGB color space.

RESULTS ON REAL AND LOW CONTRAST IMAGES

In this section, we present the results of the segmentation method applied to some images difficult to segment. These experiments consisted of segmenting color regions according to the following two steps:

1. Selection of the pixel sample. This is the only step to be left up to the user. In order to have a helpful direction for this task, the following considerations may be useful to select the number of pixels for the sample: If the color of area which the user desires to segment is solid (without additive noise), it is only necessary to have a one pixel sample from the desired area. However, if one want to take into account the lack of definition of the color happening in the borders, it is necessary to take a sample of the new colors that appear in that area due to the above condition. The pixels of the samples from the original images can be selected arbitrarily, that is, in any order, in any number and located physically adjacent or not.
2. CSI calculation. This step is automatic; its output is a gray level image showing the similarity of each pixel of the RGB true color image to the color centroid formed with the chosen pixel sample taken from the region of interest to be segmented, being white for 100% similarity and black for 0%.

The user can now threshold the CSI. This step could be necessary to obtain a template for a final segmentation of the desired color from the region of interest; it could be arranged as an automatic step using, for example, the non-supervised Otsu's threshold method.[33] This guarantees that the segmented colors are the real ones. During the thresholding of the CSI, some information may be lost that could be inconvenient. If the CSI itself is used as a template, then better segmented areas (without loss of pixels) are obtained, one for each selected color, but altered in some measure due to the intrinsically gray levels that conform the CSI.

We will show the good results obtained by the proposed color segmentation method when it is applied to low contrast color image in the following example. Figure 2 (left) shows a rather complex image of a fossil in a rock. We took a small pixel sample of the fossil area from which we obtained its corresponding CSI (Fig. 2, center). Figure 2 (right) shows the resulting image after thresholding with the Otsu method.

We show now the results of the segmentation taking into account the new definition of the achromatic zone G when it is applied to three classical color images in RGB 24-bit true color format.
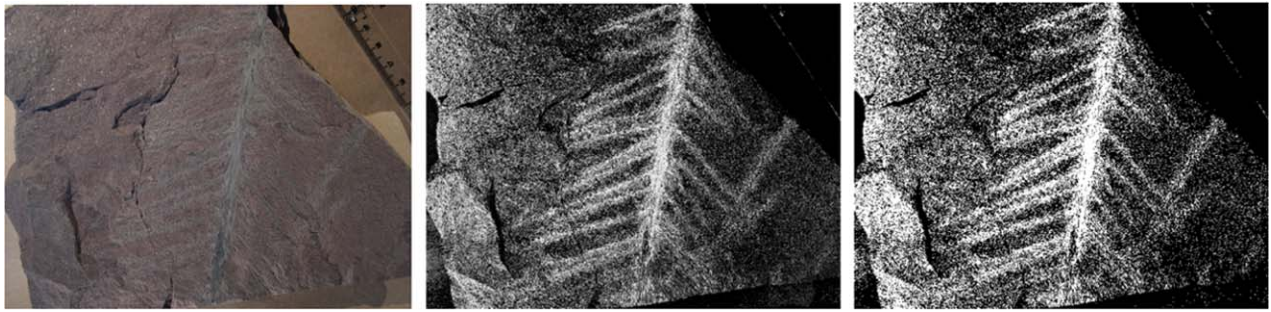
Fig. 2.   Leaf fossil in rock (left); CSI of the fossil (center); Thresholding by Otsu (right).

Figure 3 (left) shows a RGB color image (sized 200 by 200 pixels and with 33,753 different colors) of the popular baboon image; Fig. 3 (right) shows an image of horses. The images are not shown at true relative scale in order to save space.

It is possible to separate the achromatic area to obtain a better segmentation. This achromatic zone can be subdivided later using only intensity as a discriminative characteristic. The improved results of our new definition of G defined in Eq. (2) with respect to the results obtained with the common definition of that zone appearing in Refs. 2,3 are shown in Figs. 4 and 5 and Table I.

In all the composite images, the XOR logical function is used to avoid the possibility that one pixel could belong simultaneously to two different color-segmented zones or regions. Next, we demonstrate the effectiveness of the proposed color segmentation method in some relatively complex color images.

In order to evaluate the efficiency of the color segmentation method and due to the difficulty of obtaining a GT for each complex image to which the method is applied or to compare the results from different methods, the evaluation was based in these cases on the number of pixels not segmented with respect to the total number of segmented pixels in the corresponding resulting image. This ratio combines the pixels not belonging to any color cluster and those selected by two or more clusters (obtained by means of the XOR operation) with respect to the total

pixel number. It gives us a measure of the segmentation efficiency. The maximum number of selected pixels related to each color sample is always five or less. In general, the number of selected pixels for the samples depends on the complexity of the image (texture of objects), on the diversity of colors and on their spatial distribution in the image. In our experiments we do not used any preprocessing at all.

Figure 4 (left) shows in green pseudocolor those pixels which were not segmented (only four colors were selected in the process). Figure 4 (center) shows the result with the old definition of G, and Fig. 4 (right) the result with the new definition of the achromatic region G for appreciation. The improvement in quality is significant. We obtained 95.5% of pixels segmented properly (See Table I).

As another example, consider the image of two horses with shadows shown in Fig. 5 (left). Non-segmented pixels are shown in red pseudocolor. Figure 5 shows the segmentation of the achromatic zone with the former (center) and the new definition (right) of the achromatic zone G. The improvement in quality is appreciable. We obtained 97.1% of segmented pixels (See Table I).

Table I summarizes the results obtained in the segmentation of three images. The last column of Table I shows the percentage of segmented pixels obtained in these images. In all cases, the possibility that one pixel could belong to two different colors segmented zones or regions

Fig. 3.   Baboon (left); Horses (right).

Fig. 4. Composite image of five segmented colors (left), and results obtained with the old (center) and the new achromatic zone *G* (right).

has been avoided by means of the application of the XOR logical function (of two or more partial segmentations). A result with many black pixels indicates that there has been a coincidence in segmented pixels from two or more partial segmentations considered in the XOR operation.

When the results with the new achromatic region *G* are compared to those of the former definition, the difference is remarkable; whereas the new achromatic area seems segmented correctly the former one has segmented only a couple of pixels. As can be observed from Table I, the average accuracy of the color segmentation in three complex images, without an exhaustive selection of colors and a small number of pixels (4–5 on average) per color sample, is 95.91%.

We are working on obtaining the edges between segmented colors. They appear among those remaining pixels that were not segmented after all the colors of the image were selected.

While the development of segmentation algorithms has attracted remarkable consideration, relatively fewer efforts have been spent on their evaluation.[8–11] Since none of the proposed automatic segmentation algorithms published is generally applicable to all types of images and different algorithms are not equally suitable for particular applications, the performance evaluation of segmentation algorithms and its characterization are very important subjects in the study of segmentation.[9]

For a long time, the evaluation was limited to a few real images acquired from a particular application, which has the advantage that they are closer to reality although the intrinsic random nature makes them unsuitable for analytical evaluation.[8,9,12] Many undetermined characteristics of those images make them practically impossible to be used in the comparison of different segmentation techniques because many phenomena are mixed which makes it difficult to study each one's influence individually.[9] Another problem comes from the lack of a GT which has to be obtained from "experts" whose results always have intrinsic differences. This subjective and imprecise procedure is not appropriate for quantitative evaluations.[8,12]

In our case, the evaluation and characterization of a semiautomatic color image segmentation method is based on synthetic images generated with its associated GT. The synthetic images where designed to evaluate the efficiency of achieved color information from given segmentation algorithms. The system was applied to our semiautomatic color segmentation method. By the use and analysis of ROC curves and graphs, we obtained some proper characteristics of the segmentation method under study, such as its stability related to the threshold selection and to the selection of the appropriate number of pixels required by the color samples. This evaluation method may be useful for assessing the quality of the use of the color information inside the segmentation algorithms in general.

Fig. 5. Composite image of three segmented colors (left) and results obtained with the old (center) and the new achromatic zone *G* (right).

TABLE I. Results of the global segmentation per image.

No.	Image	Number of pixels in image	Number of colors (levels)	Number of colors (levels) selected	Total number of pixels used as samples	Number of non-segmented pixels	% of segmented pixels
1	Baboon	40,000	33,753	5	31	1803	95.5
2	Horses	154,401	71,727	3	14	4619	97.1

BENCHMARK TESTING

To evaluate the proposed color segmentation method, tests were performed between our system and two different classification methods implemented in the $L*a*b*$ color space[27,36]: (1) Using the minimum Euclidean distance of $a*$ and $b*$ channels rejecting $L*$ as implemented by Matlab, Ver. 2014, and (2) Using a probabilistic approach on $a*$ and $b*$ channels. The manner in which the tests were implemented is as follows:

In the case of the minimum Euclidean distance of the $a*$ and $b*$ channels in the $L*a*b*$ color space, the RGB image and the pixels samples (of object and background) were previously transformed to the $L*a*b*$ color space discarding in all cases the luminance $L*$, in order to calculate the Euclidean distance on the $a*b*$ (color information) channels independently of the illumination $L*$.

Then, the centroids (average of the values $a*$ and $b*$ of the pixel samples) representing the colors of the figure and the background in the color space $L*a*b*$ were calculated for each sample. The Euclidean distance between the centroid of each class and every pixel of the image is calculated to classify the pixels as object or background according to the minimum distance. Details can be consulted in URL http://www.mathworks.com/help/images/examples/color-based-segmentation-using-the-l-a-b-color-space.html.

In the probabilistic approach, we also transformed the image and pixels samples (of object and background) to the $L*a*b*$ color space discarding in all cases the luminance $L*$. Then, we calculated the mean and standard deviation of the values $a*$ and $b*$ from the pixel samples. From this information, we approximated normal probability functions (PDFs) of the probability of every pixel to belong to the object or background classes using Gaussians for every channel $a*$ and $b*$. Next we calculated the likelihood[26]:

$$P^i_{1/2}(x) = \frac{p^i_1(F_i)}{p^i_1(F_i) + p^i_2(F_i)} \quad (5)$$

Equation (5) expresses the likelihood[26] for the pixel x to be in the region 1 (object) with respect to p^i_1 (object) and p^i_2 (background) for a given channel F_i which can be $a*$ or $b*$ in this case; p represents a Gaussian PDF with the calculated values of mean and standard deviation. Similarly, we calculated $P^i_{1/2}(x)$. To integrate the likelihood information of the two channels $a*$ and $b*$, the likelihood function of each channel was multiplied:

$$P_{1/2}(x) = P^1_{1/2}(x) * P^2_{1/2}(x) \quad (6)$$

Similarly, we calculated $P_{1/2}(x)$. Classification comes after obtaining the maximum between them and assigning accordingly. In our case the following steps were performed:

Samples of both background and object were taken, from which centroid and standard color dispersion was calculated.

The 24-bit RGB image (true color) was transformed to our modified HSI color space.

For each pixel, the similarity function [Eq. (1)] to the centroids of object and background was calculated creating two CSI images.

Each pixel of the RGB image was classified by calculating the maximum value for each pixel position between the CSI images of the object and that of the background.

The base shape of the synthetic image to be used in our benchmark testing was created with the following features:

- Concave and convex sections in order to make it more representative of real images, such as natural flowers.
- Extreme omnidirectional curvature in the entire image to hinder obtaining the edges applying mask edge detectors.
- The object was centered in the image.

The resulting flower-shaped object in the image is considered as the object of interest and the GT in all subsequent tests (Fig. 6).

In addition to this object of interest, several features were imposed in order to hinder its color-based segmentation:
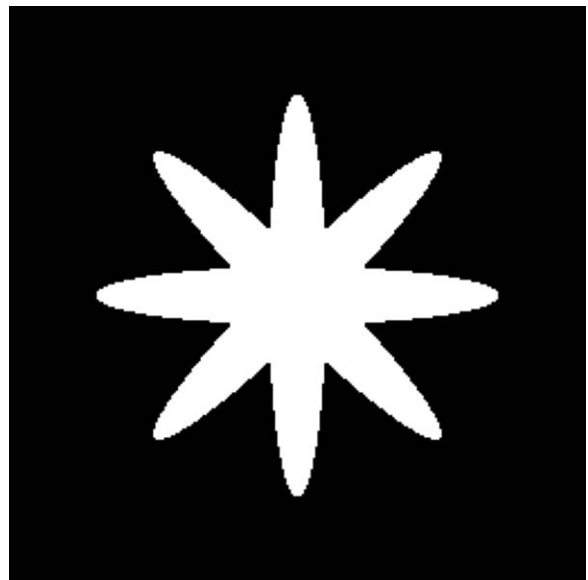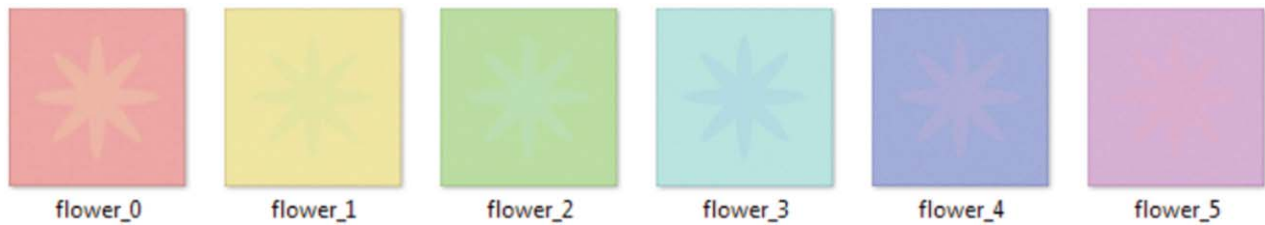

Fig. 6. Flower-shaped ground truth.

Fig. 7. Testing images with Delta in HUE.

- Low contrast. The contrast between the object and the background in all images was very low for an observer, including some in which at a glance one cannot see the difference (e.g. Flower_5 in Fig. 7).

The difference between the color characteristics of the object of interest and the background we call Delta and it occurs at different directions of the HSI color space. Tests were performed with saturation = 0.3 and Intensity = 0.5.

- Blurred edges. A mean filter of size 3×3 pixels was applied to the whole image to blur the corners and to make detection of the object more difficult; this was done before the introduction of Gaussian noise.
- Introduction of Gaussian noise with SNR value = 1. The noise was applied to each of the RGB channels individually, and later we assembled the channels to create the RGB color image with noise.

Samples of pixels corresponding to the object were obtained by two squares of 2×2 pixels starting at the pixel (84, 84) and (150, 150). Samples for background pixels were obtained by two squares of 2×2 pixels starting at pixel (15, 15) and (150, 180).

The images were generated in the sectors 0°, 60°, 120°, 180°, 240°, and 300°. To these test images, we later applied a faded shadow in increments of 10% in each step.

A shadow fading was applied to all noisy blurred images with the light center in the fixed coordinates (150,150) in images of 256×256 pixels. It was applied gradually with 10% increments at each step. Figure 8 shows in detail the fading for Flower_0.

Results and Discussion

In this section, the results are shown graphically in Fig. 9. The first position means no shadow and position 11 means 100% shadow fading. All the images had the same post-processing: elimination of areas smaller than 30 pixels and a morphological closing with a circular structuring element of radius equal to two pixels.

The results of the application of our proposed solution for the color image segmentation with a different level of shadow fading (shown in every third row of each color) compared to those obtained with the Euclidean metric of $a*$ and $b*$(every first row of each color) and the probabilistic approach in $a*$ and $b*$ (every second row of each color) are included in Fig. 8 for each color quadrant (0°, 60°, 120°, 180°, 240°, and 300°) and at 10% increments of the shadow fading.

As it can be seen from the resulting segmented images of the test images (Fig. 9 third row of each color), our system behaved correctly in all cases always segmenting the object of interest with a high hit rate of about TP 95% and with a low error rate of around 3% on average. We cannot say the same in both implementations in the $L*a*b*$ color space as the Euclidean distance or probabilistic approach in that space.

The first row of each color shows the results for classifier using the Euclidean distance of the channels $a*b*$. The second line of each color shows the results using the probabilistic classifier. As it can be seen from Fig. 9, the probabilistic approach improves in all cases the object segmentation, allowing in some cases to segment most of the object of interest in all shade levels applied as in cases such as Red 0°, yellow 60°, cyan 180°, and blue 240°, where the Euclidean distance fails. In other cases, it could not separate the object from background at high levels of shading, but there is an improvement in quality of segmenting the object at a specific level of shadow as in the case of Fig. 9 green 120° at 50% level of shadow, where the object of interest is extracted in the case of probabilistic approach but is not in the results of the minimum Euclidean distance in $a*$ and $b*$ (second and first, respectively, green 120°, Fig. 9).

As shown in the graphs of Fig. 10 and in coincidence with the visual analysis of the corresponding flower (Fig. 9), the segmentation fails with the Euclidean Distance of $a*$ and $b*$ (Fig. 10 center) and using the probabilistic approach in the $L*a*b*$ space (Fig. 10 right) starts at different levels of faded shadow, whereas our system is practically immune to the faded shadow (Fig. 10 left).
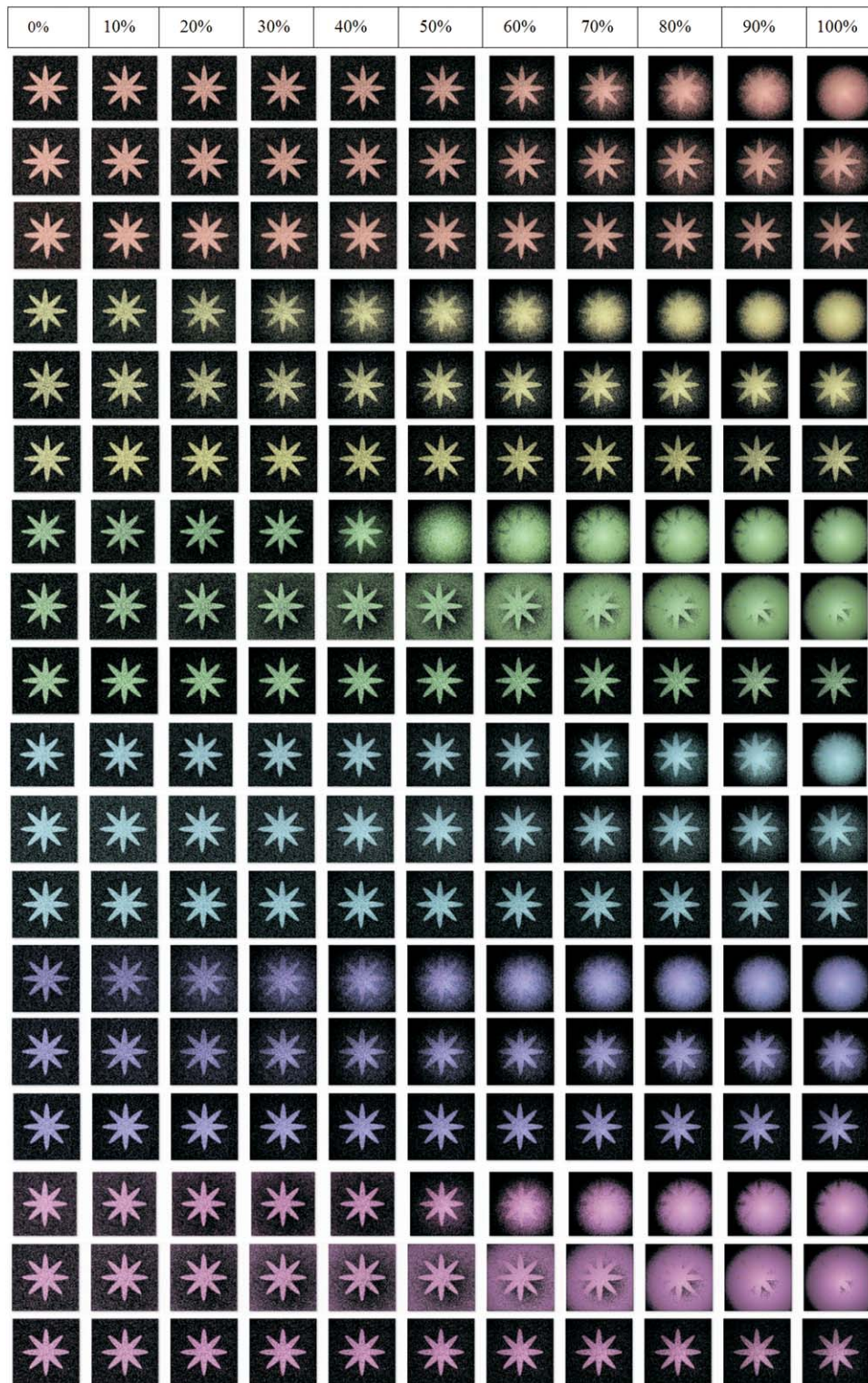

Fig. 8. Example in color quadrants with a faded shadow applied at 0°.

Fig. 9.   Results of the color segmentation achieved between the Euclidean metric of *a** and *b** parameters in the *L*a*b** color space (top rows of each color). The probabilistic approach in *a** and *b** color channels (middle rows of each color) and our solution (bottom rows of each color), for each color quadrant (0°, 60°, 120°, 180°, 240°, and 300°) at 10% increments of shadow fading in each step.

One can see three general trends in the FP behavior in Fig. 10 center: (1) later increase in an angle of approximately 45° in cases of Flower_0 and Flower_3 (with diamond marker); (2) slowly and progressively increases in cases of Flower_1 and Flower_4 (with square marker); and (3) sharply increases in cases of Flower_2 and Flower_5 (with circular marker). The behavior is repeated every 180° and coincides with the opponent color positions (yellow-blue for example).
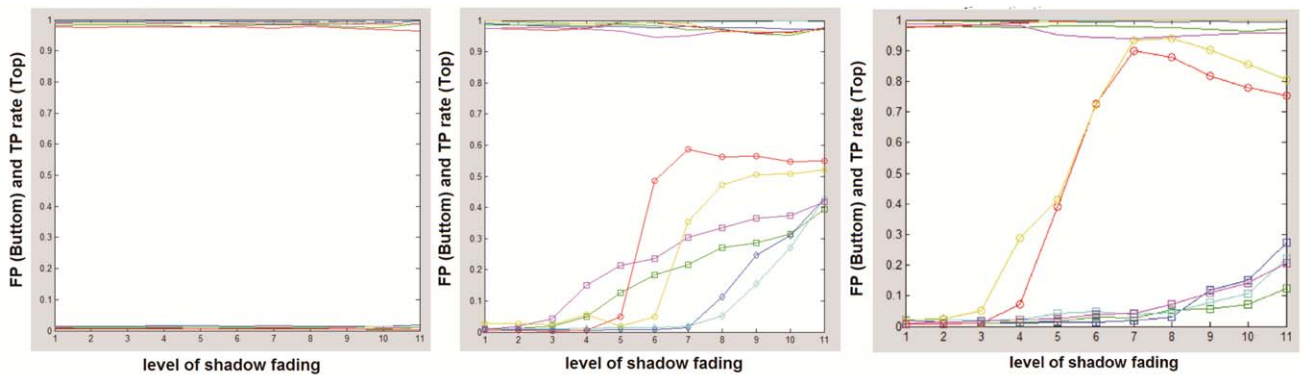
Fig. 10. Plots of our system (left), the Euclidean distance of $a*$ and $b*$ (center) and the probabilistic approach on $a*$ and $b*$ (right).

From Fig. 10, one can observe two different general trends in the FP behavior: (1) abrupt increase as in cases of Flower_2 and Flower_5; (2) slowly increase in all other cases.

The observed visually improvement in the quality of segmentation by the probabilistic approach compared to the Euclidean metric in $a*$ and $b*$ is not correctly reflected in the final graphs because the final post-processing is the same as in all tests: elimination of connected pixels lower than 30 pixels followed by a morphological closing with a circle of radius of 2 pixels as structuring element. These features can be highlighted using different post processing.

Figure 11 shows details of the curves related to TP and FP of our system with the following color code: Flower_0 (blue), Flower_1 (green), Flower_2 (red), Flower_3 (cyan), Flower_4 (purple), and Flower_5 (yellow). Variations in curves are lower than 1%. Table II shows this case and all other cases and the level when a notorious failure occurs in the color segmentation quality.

Efficiency ROC Graphs

To obtain a representative ROC curve illustrating behavior of our system compared with those implemented in the $L*a*b*$ color space in all color sectors under study, we calculated the average TP and FP for all color flowers, obtaining the results shown in Fig. 12. From the corresponding ROC curves, it can be seen that our system is maintained in the high efficiency area in all cases (coordinate 0, 1) (Fig. 12 left) while the Euclidean metric of $a*$ and $b*$ (Fig. 12 center) and the probabilistic approach (Fig. 12 right) progressively moves away from the high efficiency zone.

The results of the Euclidean metric of $a*$ and $b*$ and the probabilistic approach keep stable initially and later slowly and progressively moved to the upper right area of the ROC curve that can be thought of as the "liberal" side (coordinate 1, 1) as they make positive classifications, and, although there is weak evidence that almost all positives were classified properly, they have a high rate of non-convenient false positives (FP).
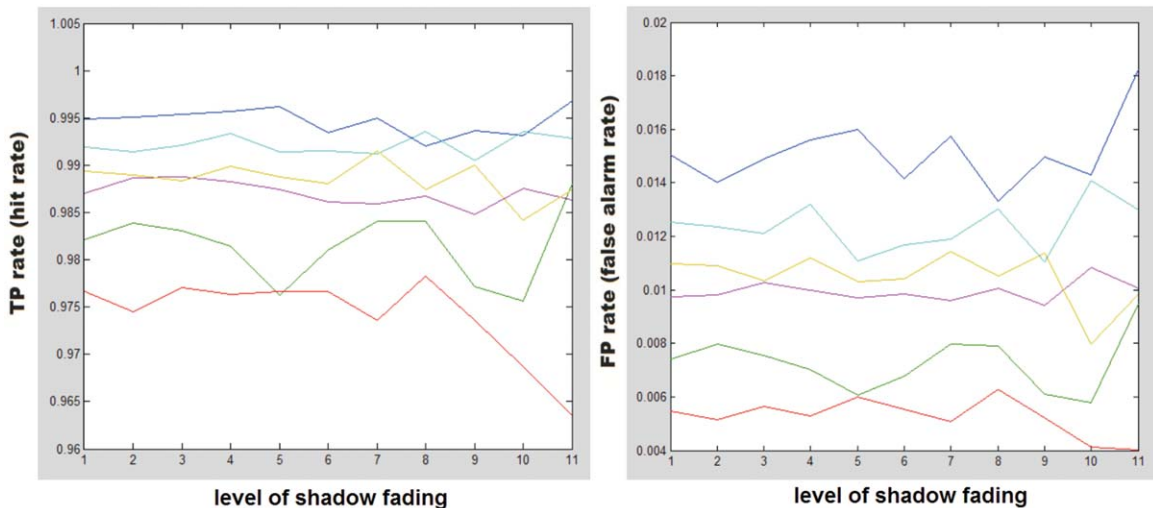

Fig. 11. Details of TP (left) and FP (right) of our system.

TABLE II. Observations concerning the behavior of the plot curves comparing our system with the other two.

Flower	Line Color	Euclidean metric of a^* and b^*	Probabilistic approach on a^* and b^*	Color adaptive similarity function
0	Blue	60% (position 7) Increases at 45°	70% (position 8) Increases slowly	Immune
1	Green	30% (position 4) Increases slowly and progressively	80% (position 9) Increases slowly	Immune
2	Red	40% (position 5) Sharply increases	30% (position 4) Sharply increases	Immune
3	Cyan	70% (position 8) Increases at 45°	80% (position 9) Increases slowly	Immune
4	Purple	20% (position 3) Increases slowly and progressively	70% (position 8) Increases slowly	Immune
5	Yellow	50% (position 6) Sharply increases	20% (position 3) Sharply increases	Immune

CONCLUSIONS

The results achieved in this article demonstrate that the adaptive color similarity function and the presented supervised color segmentation method presented offers a useful and efficient alternative for the segmentation of objects (or regions) with different colors in relatively complex color images with good performance in the presence of unavoidable additive noise. The method discriminates whichever type of different color objects independently from their shapes and tonalities in a very straightforward way. The average accuracy of the color segmentation in three complex images, without an exhaustive selection of colors and a small number of pixels (4–5 on average) per color sample, was 95.91%.

Conversely, a quantitative evaluation and characterization of the proposed adaptive color similarity function and a semiautomatic color image segmentation algorithm directly obtained from the similarity function has been presented. It was carried out by generating synthetic images each with its corresponding GT image. The true positive rate (TP rate) and false positive rate (FP rate) for every image was calculated to obtain ROC curves of the results. This system is useful in general for assessing the quality of the use of the color information inside segmentation algorithms.

Behavior was assessed by varying size, shape and color contrast, amount of additive noise, threshold, and number of pixels taken in the sample. After an analysis of the corresponding ROC curves, the algorithm showed good performance in most cases with TP rate greater than 95% and FP rate lower than 0.2%. The ROC curve for color contrast shows a good performance of the algorithm even in the cases where the color contrast is rather low meaning that for a normal observer it is difficult to find any color difference. It is shown that the characterization of the achromatic region presented in this article improves the performance in comparison to the published methods due to the affectation of saturation by an exponential factor in an effort to model the human visual response better in the case of very low or very high brightness. The improvement in quality of its results is significant.

A comparative study between the behavior of the proposed method and two comparable segmentation techniques in color images is presented using (1) the Euclidean metric of the a^* and b^* color channels rejecting L^* in the CIE $L^*a^*b^*$ color space and (2) a probabilistic approach on a^* and b^*.

Regarding the evaluation of the color segmentation method in really difficult conditions, it is shown that our method performed well in all tests and remained close to the high efficiency zone of the ROC curves (coordinates 0,1) without noticeable changes, while increasing the level of faded shadow as shown in the corresponding curves. The segmentation algorithm using the CIE $L^*a^*b^*$ color space and discarding L^* when calculating the Euclidean distance, suffered from errors in all cases. It manifested in different degrees and at different levels of faded shadow (less than 10% to 80%). Three types of
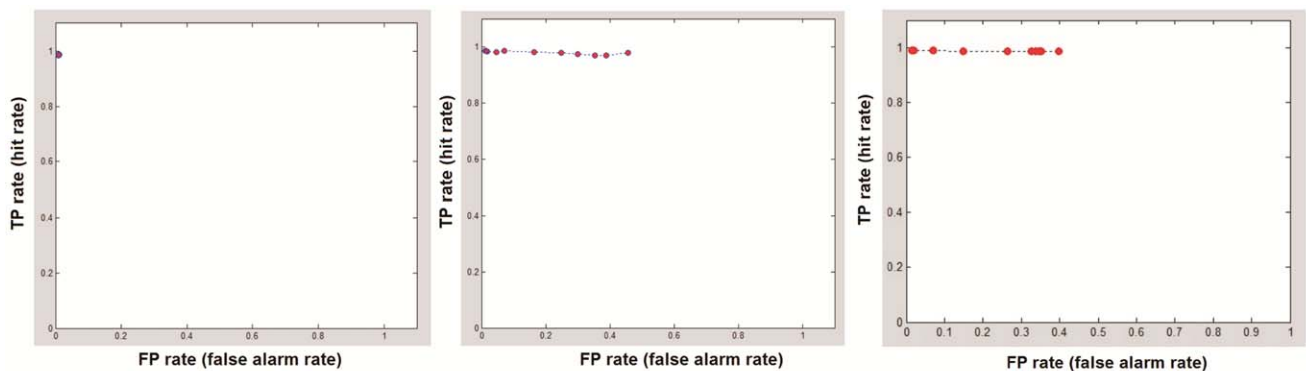

Fig. 12. ROC curve of our system (left), of the Euclidean metric of a^* and b^* for all Flowers (center) and of the probabilistic approach on a^* and b^* for all Flowers.

trends can be noticed in sectors with 120° of difference: (1) rise of the curve abruptly (Flowers_0, _2 and _4 which corresponds to the R G B color channels) with high sensibility to the faded shadow (higher than RGB); (2) slow Rise (Flowers_1 and_5) lower than RGB; and (3) insensitive increment at near 90% (Flower_3).

The segmentation method using a probabilistic approach improved in many cases the results using the Euclidean metric but in some other cases it could not obtain good results due to corruption of the $L*a*b*$ color space.

As it can be seen from the results, our adaptive color similarity function in all cases exceeded: (1) The Euclidean distance in color space $L*a*b*$ but discarding $L*$ and (2) the probabilistic approach on $a*$ and $b*$ channels. The proposed adaptive color similarity function performed well in all cases with rates higher than 95% of TP and FP rate less than 0.2% on average.

It can be noticed that the non-consideration of the luminance parameter $L*$ in calculating Euclidean distance (in each pixel of the object or of the background) and in the probabilistic approach did not made the methods immune to changes in lighting; so simple shadow can alter the quality of their results. It can also be noticed from the results that the parameters $a*b*$ from the color space $L*a*b*$ are not independent of the $L*$ parameter as one might suppose.

Our segmentation method can also be used directly in grayscale images without making any changes, achieving good results. On the contrary, the other tested methods that use the $L*a*b*$ color space need to include the luminance $L*$ to perform the segmentation, since $a*$ and $b*$ values remain unchanged in the center of $a*b*$ plane. An additional task is to decide when the luminance $L*$ must be considered in calculating the Euclidean distance.

Our testing system can be used either to explore the behavior of a similarity function in different color spaces or to explore different similarity metrics (or similarity functions) in the same color space. Instead of exchanging color spaces in the experiments, it would only be necessary to exchange the metric or the similarity function.

In future work, we would like to evaluate different color zones of different saturations, grayscale images, and with Delta saturation among others. Our testing system can be used either to explore the behavior of a similarity function (or metric) in different color spaces or to explore different metrics (or similarity functions) in the same color space.

1. Gonzalez, RC, Woods, RE. Digital Image Processing, 3rd edition. Upper Saddle River, NJ: Prentice Hall; 2008. 954 p.

2. Plataniotis, KN, Venetsanopoulos, AN. Color Image Processing and Applications, 1st edition. Berlin Heidelberg Germany: Springer; 2000. 354 p.

3. Alvarado-Cervantes R. Segmentación de patrones lineales topológicamente diferentes, mediante agrupamientos en el espacio de color HSI. M. Sc. Thesis, Mexico: Center for Computing Research, National Polytechnic Institute; 2006.

4. Cheng H, Jiang X, Sun Y, Wang J. Color image segmentation: Advances and prospects. Pattern Recognit 2001; 34:2259–2281.

5. Angulo J, Serra J. Modelling and segmentation of colour images in polar representations. Image Vis Comput 2007; 25: 475–495.

6. Hanbury, A, Serra, J. A 3D-polar coordinate colour representation suitable for image analysis. Technical Report PRIP-TR-77, Vienna Austria: Pattern Recognition and Image Processing Group, Institute of Computer Aided Automation, Vienna University of Technology, 2003.

7. Poynton C. Frequently Asked Questions about Gamma. Available at: http://www.poynton.com/PDFs/GammaFAQ.pdf; 2002. The URL was last visited on May 10, 2016.

8. Zhang H, Fritts JE, Goldman SA. Image segmentation evaluation: A survey of unsupervised methods. Comput Vis Image Underst 2008; 110:260–280.

9. Zhang YJ. A survey on evaluation methods for image segmentation. Pattern Recognit 1996; 29: 1335–1346.

10. Zhang, YJ. A review of recent evaluation methods for image segmentation. Proceedings of the 6th International Symposium on Signal Processing and Its Applications, Kuala Lumpur, 2001. p 148–151.

11. Zhang YJ. A summary of recent progresses for segmentation evaluation. In: Zhang YJ, editor. Advances in Image and Video Segmentation. IGI Global Research Collection, Idea Group Inc (IGI), 2006. p 423–439.

12. Zhang YJ, Gerbrands JJ. On the design of test images for segmentation evaluation. Proceedings EUSIPCO, Vol. 1; 1992. p 551–554.

13. Fawcett T. An introduction to ROC analysis. Pattern Recognit Lett 2006; 27:861–874.

14. Angulo J, Serra J. Mathematical morphology in color spaces applied to the analysis of cartographic images. GEOPRO'03: Proceeding of GEO-PRO'03, International Workshop of Semantic Processing of Spatial Data. México; 2003, 8 pages, ISBN: 970-36-0111-1.

15. Huang R, Sang N, Luo D, Tang Q. Image segmentation via coherent clustering in L*a*b* color space. Pattern Recognit Lett 2011; 32:891–902.

16. Vaitkus M, Várady T. Grayscale and color image segmentation using computational topology. Proceedings of the 17th Central European Seminar on Computer Graphics, CESCG 2013; 2013. p 1–8.

17. Gupta S, Bhuchar K and Sandhu PS. Implementing color image segmentation using biogeography based optimization. International Conference on Software and Computer Applications, IPCSIT, Vol. 9, IACSIT Press, Singapore 2011. p 79–86.

18. Sengur A, Guo Y. Color texture image segmentation based on neutrosophic set and wavelet transformation, Comput Vis Image Underst 2011; 115: 1134–1144.

19. Yue XD, Miao DQ, Zhang N, Cao LB, Wu Q. Multiscale roughness measure for color image segmentation. Inform Sci 2012; 216: 93–112.

20. Puranik P, Bajaj P, Abraham A, Palsodkar P, Deshmukh A. Human perception-based color image segmentation using comprehensive learning particle swarm optimization. J Inform Hiding Multimed Signal Process 2011; 2:227–235.

21. Celik T, Tjahjadi T. Unsupervised colour image segmentation using dual-tree complex wavelet transform. Comput Vis Image Underst 2010; 114:813–826.

22. Bourbakis N, Yuan P, Makrogiannis S. Object recognition using wavelets, L-G graphs and synthesis of regions. Pattern Recognit 2007; 40: 2077–2096.

23. Shi L, Funt B. Quaternion color texture segmentation. Comput Vis Image Underst 2007; 107:88–96.

24. Correa-Tome FE, Sanchez-Yanez RE, Ayala-Ramirez V. Comparison of perceptual color spaces for natural image segmentation tasks. Opt Eng 2011; 50:117203

25. Martin D, Fowlkes C, Tal D, Malik J. A database of human segmented natural images and its application to evaluating segmentation algorithms and measuring ecological statistics. Proceedings of the 8th International Conference on Computer Vision, Vol. 2, Vancouver, BC, 2001. p 416–423.

26. Protiere A, Sapiro G. Interactive image segmentation via adaptive weighted distances. IEEE Trans Image Process 2007; 16:1046–1057.

27. Bai, X, Sapiro, G. A geodesic framework for fast interactive image and video segmentation and matting. IEEE 11th International Conference on Computer Vision, Rio de Janeiro, 2007. p 1–8.

28. Rother C, Kolmogorov V, Blake A. Grabcut: Interactive foreground extraction using iterated graph cuts. ACM Trans Graph 2004; 23: 309–314.

29. Kim C, You BJ, Jeong MH, Kim H. Color segmentation robust to brightness variations by using B-spline curve modeling. Pattern Recognit 2008; 41:22–37.

30. Harun NH, Mashor MY, Mokhtar NR, Aimi Salihah AN, Hassan R, Raof RAA, Osman MK. Comparison of acute leukemia image segmentation using HSI and RGB color space. 10th International Conference on Information Science, Signal Processing and their Applications, ISSPA 2010, Kuala Lumpur, 10–13 May 2010. p 749–752.

31. Macaire L, Vandenbroucke N, Postaire JG. Color Image segmentation by analysis of subset connectedness and color homogeneity properties. Comput Vis Image Underst 2006; 102:105–116.

32. Chabrier S, Laurent H, Rosenberg C, Zhang YJ. Supervised evaluation of synthetic and real contour segmentation results. 14th European Signal Processing Conference, EUSIPCO 2006, Florence, Italy, September 2006. p 1–4.

33. Otsu N. A threshold selection method from gray-level histograms. IEEE Trans Syst Man Cybern 1979; 9:62–66.

34. Sezgin M, Sankur B. Survey over image thresholding techniques and quantitative performance evaluation. J Electron Imaging 2003; 13: 146–165.

35. Alvarado-Cervantes R, Felipe-Riveron EM. Refined achromatic zone segmentation in color images. In: Castillo Montiel E, Chimal Eguía JC, Uriarte Arcia A, Cabrera Rivera L, editors. Advances in Computer Science, Vol. 58. 12th Conference on Computing, CORE 2012. México: CIC IPN; 2012. p 79–90.

36. Matlab v 7.10.0.499: Image Processing Toolbox, Color-Based Segmentation Using K-Means Clustering (R2010a). http://www.ics.uci.edu/~dramanan/teaching/ics273a_winter08/projects/avim_report.pdf (The URL was last visited on May 10, 2016).